JGR Biogeosciences

RESEARCH ARTICLE
10.1029/2024JG008445

Organic Matter Composition Versus Microbial Source: Controls on Carbon Loss From Fen Wetland and Permafrost Soils

Sommer F. Starr[1], Kimberly P. Wickland[2], Anne M. Kellerman[1], Amy M. McKenna[3,4], Martin R. Kurek[1], Aubrey Miller[1], Ariana Katsaras[1], Thomas A. Douglas[5], Rachel Mackelprang[6], Ashley L. Shade[7], and Robert G. M. Spencer[1]

[1]Department of Earth, Ocean, and Atmospheric Science, National High Magnetic Field Laboratory Geochemistry Group, Florida State University, Tallahassee, FL, USA, [2]Geosciences and Environmental Change Science Center, United States Geological Survey, Boulder, CO, USA, [3]National High Magnetic Field Laboratory FT-ICR MS Group, National High Magnetic Field Laboratory, Tallahassee, FL, USA, [4]Department of Soil and Crop Sciences, Colorado State University, Fort Collins, CO, USA, [5]U.S. Army Engineer Research and Development Center, Cold Regions Research and Engineering Laboratory, Ft. Wainwright, AK, USA, [6]California State University, Northridge, CA, USA, [7]Laboratoire d'Ecologie Microbienne, UMR CNRS 5557, UMR INRAE 1418, Universite Claude Bernard Lyon 1, VetAgro Sup, Villeurbanne, France

Abstract Wetland and permafrost soils contain some of Earth's largest reservoirs of organic carbon, and these stores are threatened by rapid warming across the Arctic. Nearly half of northern wetlands are affected by permafrost. As these ecosystems warm, the cycling of dissolved organic matter (DOM) and the opportunities for microbial degradation are changing. This is particularly evident as the relationship between wetland and permafrost DOM dynamics evolves, especially with the introduction of permafrost-derived DOM into wetland environments. Thus, understanding the interplay of DOM composition and microbial communities from wetlands and permafrost is critical to predicting the impact of released carbon on global carbon cycling. As little is understood about the interactions between wetland active layer and permafrost-derived sources as they intermingle, we conducted experimental bioincubations of mixtures of DOM and microbial communities from two fen wetland depths (shallow: 0–15 cm, and deep: 15–30 cm) and two ages of permafrost soil (Holocene and Pleistocene). We found that the source of microbial inoculum was not a significant driver of dissolved organic carbon (DOC) degradation across treatments; rather, DOM source and specifically, DOM molecular composition, controlled the rate of DOC loss over 100 days of bioincubations. DOC loss across all treatments was negatively correlated with modified aromaticity index, O/C, and the relative abundance of condensed aromatic and polyphenolic formula, and positively correlated with H/C and the relative abundance of aliphatic and peptide-like formula. Pleistocene permafrost-derived DOC exhibited ~70% loss during the bioincubation driven by its initial molecular-level composition, highlighting its high bioavailability irrespective of microbial source.

Plain Language Summary As the Earth warms, wetlands and permafrost in the Arctic are thawing, releasing large amounts of stored carbon into the atmosphere. To understand how organic matter composition and the source of microbes from either wetlands or permafrost deposits impacts the degradation of carbon released from these systems, we mixed wetland and permafrost soil leachates and analyzed carbon loss and organic matter composition changes over one hundred-day laboratory incubations. We found that the type of soil had a bigger impact on the breakdown rate than the source of the microbial inocula. Soil leachates that were richer in certain carbon molecules were broken down faster. Carbon from Pleistocene-age permafrost soil was particularly susceptible to degradation, showing ~70% loss over time. This study helps us understand how climate change might affect the amount of carbon released from thawing wetlands and permafrost.

Key Points:

- Dissolved organic matter (DOM) composition is a primary factor controlling its biodegradability in wetland and permafrost environments
- The source of microbial community had a limited impact on biodegradable dissolved organic carbon loss during experimental 100-day incubations
- Pleistocene permafrost-derived DOM is highly susceptible to microbial degradation, indicating a significant potential for greenhouse gas production upon thaw

Supporting Information:

Supporting Information may be found in the online version of this article.

Correspondence to:

S. F. Starr,
sommerstarr@trentu.ca

Citation:

Starr, S. F., Wickland, K. P., Kellerman, A. M., McKenna, A. M., Kurek, M. R., Miller, A., et al. (2025). Organic matter composition versus microbial source: Controls on carbon loss from fen wetland and permafrost soils. *Journal of Geophysical Research: Biogeosciences*, *130*, e2024JG008445. https://doi.org/10.1029/2024JG008445

Received 3 SEP 2024
Accepted 14 APR 2025

1. Introduction

The Arctic is warming at twice the global average rate and is experiencing rapid and drastic changes to its ecology, hydrology, and biogeochemistry as a result (Druckenmiller et al., 2022; Klanten et al., 2023; Phoenix & Treharne, 2022; Walvoord et al., 2016). Critically, northern wetland and permafrost soils represent some of the most significant reservoirs of organic carbon (OC) globally, and continued warming is projected to mobilize

hundreds of Pg of previously frozen C into the environment over the next century (Miner et al., 2022; Natali et al., 2021; Schuur et al., 2022). As these soils warm, much of this OC is expected to enter surface waters as dissolved organic carbon (DOC) where it becomes available for a host of biogeochemical roles including microbial processing and ultimately export to the Arctic Ocean (Holmes et al., 2013; Kicklighter et al., 2013; Spencer et al., 2015; Starr et al., 2023).

Climate change will not only impact DOC concentration across Pan-Arctic watersheds but will also change the composition and thus processing of exported dissolved organic matter (DOM) (Behnke et al., 2021; Frey & McClelland, 2009; Starr et al., 2023). Arctic watersheds transport approximately 35 Tg of DOC annually to the Arctic Ocean (Starr et al., 2023; Vonk et al., 2015), with a range of contributing sources and DOM chemical composition that closely reflects the terrestrial attributes of the watersheds. It is critical to understand how the DOM composition of inputs into aquatic ecosystems from vulnerable OC stocks influences the processing and fate of these inputs across different landscapes. Biodegradable DOC (BDOC) in particular is an important substrate for heterotrophic processing and is subsequently a foundational component of ecosystem metabolism (Vonk et al., 2015). DOM composition has been shown to directly affect its availability for biodegradation; typically, DOM with lower molecular weight, higher H/C ratios, and lower O/C ratios is more bioavailable, while DOM comprised of higher molecular weight compounds with greater aromaticity is more stable with respect to biodegradation on relatively short time scales (Behnke et al., 2021; Jiao et al., 2010; Sun et al., 1997). The source and age of DOM influences its composition and, subsequently, its biodegradability (Wickland et al., 2007, 2018) but yet little is known with respect to how important microbial community structure or source is in controlling DOM biodegradation.

Permafrost covers 60%–80% of the Pan-Arctic watershed and exerts strong controls on watershed DOM dynamics where it occurs (Frey & Smith, 2005; Pokrovsky et al., 2015; Speetjens et al., 2023). Permafrost-derived DOM may be subject to degradation from photochemical and microbial processes. BDOC loss from permafrost-derived inputs is typically rapid and strongly influenced by its unique composition; that is, high relative abundance (RA) of aliphatic formula with elevated H/C ratios and low molecular weight organic acid concentrations (Drake et al., 2015; Ewing, O'Donnell, et al., 2015; Ewing, Paces, et al., 2015; Spencer et al., 2015). This BDOC loss has been observed to be as high as 50% within just 1 week after experimental thawing of Pleistocene-aged deposits (Drake et al., 2015; Spencer et al., 2015; Vonk et al., 2015). Discontinuous permafrost is especially vulnerable to thaw, which includes many Pleistocene-aged, organic-rich deposits, and this thaw influences DOC dynamics through changing hydrology and the release of ancient DOC formed under anoxic conditions to surrounding aquatic environments (Ewing, O'Donnell, et al., 2015; Ewing, Paces, et al., 2015; Moore et al., 2023; Schuur et al., 2008; Tank et al., 2020). Importantly, nearly half of northern wetlands are influenced by permafrost (Hugelius et al., 2020), creating the potential for DOC mobilization from underlying permafrost laterally into wetland soils as warming continues to increase the thickness of the active layer. The mobilization of ancient carbon into oxidizing environments has implications for the global carbon cycle, as rapid degradation of previously stored DOM may increase greenhouse gas flux to the atmosphere and contribute to greater warming through climate feedbacks.

Like permafrost, northern wetlands have historically functioned as important long-term carbon sinks, but Arctic wetlands are also hotspots for OC transformation and significant DOC contributors to aquatic ecosystems. The abundance and OC cycling capacity of Arctic wetlands is expected to change with further shifts in climate (Chaudhary et al., 2020; Kicklighter et al., 2013; Perreault et al., 2017; Takano et al., 2021). Wetland DOM has been observed to be relatively stable to biodegradation and is comprised mainly of plant-derived polysaccharides, with large relative contributions from phenolic and aromatic compounds (D'Andrilli et al., 2010; Hodgkins et al., 2016; Tfaily et al., 2013). While it has been suggested that permafrost-derived DOM subsidies will be rapidly mineralized in wetland, rivers, and lakes under continued warming (Drake et al., 2015; Mohammed et al., 2022), northern wetlands have also been attributed as providing protective effects against warming-related permafrost DOM subsidies through direct storage as peat accumulation (Heffernan et al., 2020; Holmes et al., 2022) or through indirect geochemical controls (Tanentzap et al., 2021). Other studies have suggested that the fate of terrestrial OC in wetland systems following permafrost thaw is difficult to predict due to variability in redox conditions and the variable processing rates of the highly heterogenous mixture of compounds that contribute to DOM in these systems (Harden et al., 2008; Turetsky, 2004). Additionally, to our knowledge, there have not been any studies of how DOM transported in the opposite direction, from wetlands to areas of permafrost thaw, will be processed by microbial communities in permafrost soils.

The interaction between permafrost and wetland sources is complex, especially given that more than half of northern wetlands are affected by permafrost. Understanding how DOM composition and microbial communities impact and are impacted by interactions between permafrost- and wetland-derived DOM transport needs to be explicitly investigated. To explore these interactions as they may occur where DOM and microbes from warming permafrost and wetland soils may meet on the landscape under future warming conditions, we leached soils from two depths (shallow: 0–15 cm, and deep: 15–30 cm) of an Alaskan fen wetland, and two depths/ages (Holocene: approximately 2,000–3,000 years old, and Pleistocene: approximately 40,000 years old) of permafrost in order to experimentally mix DOM and microbial communities from each of the four soil sources. Given the established link between permafrost age and DOM biodegradability, we selected Pleistocene and Holocene-aged permafrost to test this relationship under our experimental conditions. Two depths were chosen for wetland soils as vertical stratification of DOC concentration and DOM composition has been well documented in peat soils and porewater (Chanton et al., 2008; Tfaily et al., 2018). We also sought to better elucidate the degradation of BDOC over relatively long-term timelines by incubating the mixtures for 100 days, as many bioincubation experiments using DOM sourced from permafrost soils have been limited to four to 8 weeks (Ni & Li, 2023; Spencer et al., 2015; Vonk et al., 2015; Zhou et al., 2019). DOC concentration was measured at seven timepoints and molecular-level composition of DOM was analyzed using Fourier Transform Ion Cyclotron mass spectrometry (FT-ICR MS) at 21 T, arguably the highest resolution technique for DOM compositional assessment available. FT-ICR MS analyses were undertaken at the beginning and end of the bioincubations to determine how initial DOM composition impacts BDOC in the bioincubations, and to assess how DOM composition changes throughout the bioincubations.

We hypothesized that the initial DOM composition from each source would influence the rate of BDOC loss over the course of the bioincubations, and that the microbial communities from each soil source would affect BDOC loss of different sources of DOM at different rates. Specifically, we hypothesized that aliphatic-enriched DOM from Pleistocene permafrost deposits would be more susceptible to microbial degradation than the more aromatic-rich DOM derived from Holocene permafrost and wetland soils, and that the microbial inocula from the relatively more biologically active wetland soils would result in more rapid BDOC loss in the Pleistocene permafrost derived leachates than permafrost derived inocula.

2. Methods

2.1. Study Site, Sample Collection, and Experimental Bioincubation Design

Soil was collected from three subsites from a wetland near Big Trail Lake (64.913534°N, −147.824063°W), Fairbanks, Alaska. Big Trail Lake is a thermokarst lake situated within fen-covered Pleistocene-aged soils (Elder et al., 2021; Walter Anthony et al., 2018, 2021). Following the convention of Kuhn et al. (2021), we define a fen here as a groundwater-fed wetland with at least 40 cm of peat formation and hydrological connectivity to surrounding soils. Soils were collected from the upper 30 cm of the fen using a knife and shovel in late June 2021. Permafrost was not present at this depth at the time of collection; thus the term "wetland soils" used hereafter are defined as being fen-derived sediments unaffected by permafrost. Surface vegetation was removed and soils were partitioned into 0–15 cm (shallow wetland soil) and 15–30 cm (deep wetland soil) sections and sealed in plastic bags and frozen.

The term "permafrost soils," used in this manuscript to describe our experimental stock types, refers to Holocene and Pleistocene-aged permafrost material used to create the respective leachates. These samples were collected from the U.S. Army Cold Regions Research and Engineering Laboratory Permafrost Tunnel Research Facility located near Fairbanks, Alaska (64.951°N, 147.621°W). Cores were extracted by dry-drilling using a Snow, Ice, and Permafrost Research Establishment (SIPRE) corer with an 8 cm diameter barrel. Holocene permafrost was collected from above the tunnel at a depth of 1–1.5 m. The collected Holocene material originates from silt that froze both epigenetically and syngenetically and is mainly ice-poor with small ice wedges (Kanevskiy et al., 2022). We estimate these samples to be 2,000–3,000 years in age based on a sediment deposition rate of approximately 0.5 mm/yr (Johnson & Lorenz, 2000). Pleistocene-aged yedoma material was accessed from inside the tunnel 80 m from the portal and collected at a depth of 16–16.5 m. Yedoma is defined as being both ice- and organic-rich permafrost that is syngenetic in origin with large ice wedges, formed in cold and dry grasslands during the Pleistocene (Kanevskiy et al., 2022). Cores were collected by drilling at a diagonal where the tunnel wall meets the floor. Past studies have estimated permafrost age in this zone of the tunnel to be approximately

33,000 years using radiocarbon dating (Mackelprang et al., 2017), having formed from silt deposited under unglaciated, eolian conditions (Hamilton et al., 1988). Since then, the tunnel floor was dropped as part of an expansion effort and samples collected for this study were approximately 3 m below the previously dated section. We estimate these deeper samples to be approximately 40,000 years in age. The collected material was shipped on dry ice and stored at −20°C.

For Pleistocene and Holocene samples, surface material that contacted the core barrel was removed in a room dedicated to processing permafrost samples. Laboratory personnel wore autoclaved laboratory coats, sterile gloves, N95 masks, hair coverings, and goggles. The outer ∼3 cm of each core was removed using a wet tile saw (without water) running sterilized 10" continuous-rim diamond blades that were changed frequently. The saw stage was covered with autoclaved aluminum foil that was replaced regularly. To homogenize samples, core sections were placed into three nested whirl-pak bags to provide a triple layer of protection. They were then placed in a tray nested in a larger tray containing blue ice packs. Bags were covered with several sterile bench underpads and struck with a rubber mallet until aggregates were approximately 1 cm in diameter.

Leachates were created by mixing each of the four types of frozen soil in their own individual Nalgene carboy with water (buffered with 0.001 N $NaHCO_3$) in a 1:4 ratio of soil to water by mass. After 24 hr of leaching at 22°C, leachates were then filtered through 1.6 μm pre-combusted glass fiber filters (450°C > 5 hr) to remove large particulates. The portions of leachate filtered to this level are referred to hereafter as "inocula." Post 1.6 μm filtration, the majority of the leachate was then subsequently filtered through pre-combusted 0.2 μm filters to remove the majority of microbial biomass; leachates filtered at this level are hereafter referred to as "stocks."

For each treatment, a 1:100 inoculum to stock solution by volume was created and transferred to either triplicate 40 mL pre-combusted (550°C > 5 hr) glass vials with 10 mL of headspace for DOC concentration analysis, or 100 mL in 125 mL Nalgene containers for FT-ICR MS. All samples were incubated in the dark at 20°C to isolate biodegradation from any effects of photochemical degradation and shaken periodically until collection on days 0, 2, 7, 14, 28, 58, or 100 of the incubation ($n = 336$). The temperature and aerobic nature of these conditions were chosen to emulate oxygenated surface waters under climate change, that is, a river or stream where water transporting microbes and DOM from both thawing permafrost deposits and wetland soils may promote interaction between these parameters on the landscape under future warming conditions. At each timepoint, the DOC samples were immediately filtered and acidified to pH 2 using HCl and stored at 4°C until DOC analysis. The FT-ICR MS samples were filtered through 1.6 μm pre-combusted glass fiber filters at each timepoint and frozen and stored at −20°C until solid phase extraction and analysis for FT-ICR MS ($n = 32$). A graphical representation of the experimental design is presented in Figure 1.

2.2. Dissolved Organic Carbon Analysis and BDOC Loss Calculations

Filtered and acidified samples were analyzed for DOC using a Shimadzu high-temperature catalytic oxidation total OC analyzer (TOC-L CPH). DOC concentrations were calculated following established protocols as in Johnston et al. (2018). BDOC loss was calculated as the percent difference in average DOC concentration between day 0 and day 100 for each individual treatment combination. To assess decay rate, a three parameter exponential decay model was fitted using the function:

$$C(t) = C\infty + z_0 e^{-kt}$$

where $C(t)$ = the modeled value at time (t); $C\infty$ = an adjustable parameter that represents the non-bioavailable component (i.e., the DOC concentration remaining at time equals infinity); z_0 = an adjustable parameter that represents the bioavailable component at time = 0; k = the first order rate constant representing the rate of DOC loss (d^{-1}), t = the time (days) and e is the base of the natural logarithm.

2.3. Solid Phase Extraction and FT-ICR MS

DOM was isolated via solid phase extraction on individual prepared 100 mg PPL cartridges (Agilent Technologies). Cartridges were prepared following established methodology (Starr et al., 2023); that is, two repetitions of soaking with HPLC grade methanol (Sigma-Aldrich Chemical Co., St. Louis, MO) for at least 4 hours before rinsing the soaked cartridges with ultrapure water twice. Bioincubation samples were acidified to pH 2 with 12 M

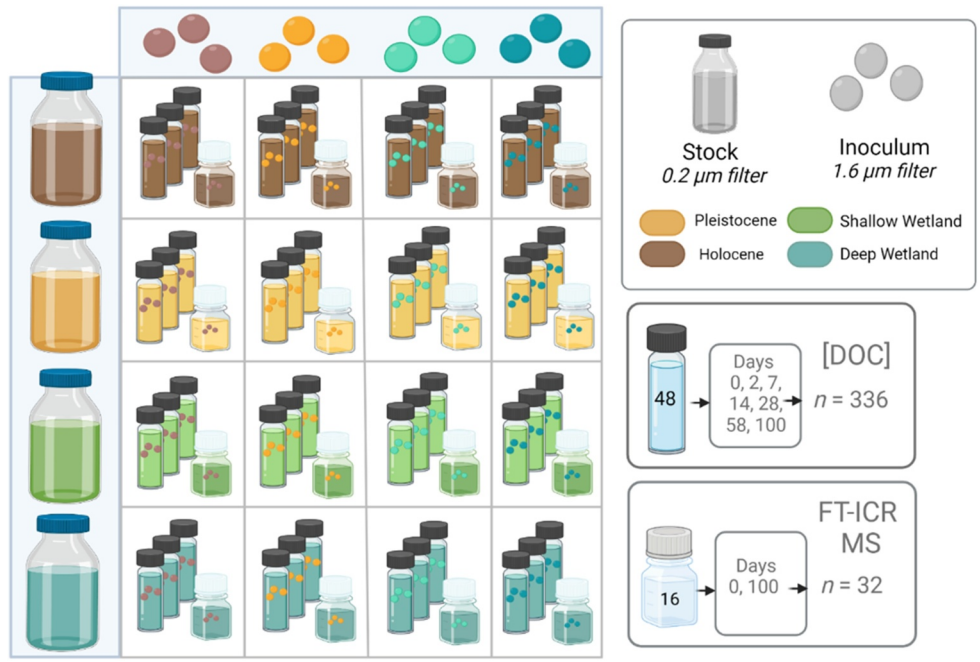

Figure 1. Experimental design. A 1:100 inocula to stock solutions were created (16 treatments) and transferred to triplicate 40 mL glass vials for dissolved organic carbon concentration analysis at seven timepoints (n = 336) or to 125 mL Nalgene containers for FT-ICR MS analysis of dissolved organic matter composition at the initial and final incubation timepoints (n = 32).

HCl, and aliquots equivalent to 40 µg C were extracted onto prepared cartridges. DOM extracted onto the cartridges was then eluted with HPLC grade methanol into pre-combusted (>550°C for 5 hr) vials to a final concentration of 40 µg OC mL^{-1} (Dittmar et al., 2008). Eluted samples were kept at −20°C prior to analysis.

DOM extracts were analyzed with a custom-built hybrid linear ion trap FT-ICR MS equipped with a 21 T superconducting solenoid magnet (Hendrickson et al., 2015; Smith et al., 2018) where the dynamically harmonized ICR cell was operated with 6 V trapping potential (Boldin & Nikolaev, 2011; Kaiser et al., 2013). Sample solution was infused via microelectrospray (50 µm i.d. fused silica emitter) at 500 nL/min by a syringe pump (Emmett et al., 1998). Typical conditions for negative ion formation were as follows: emitter voltage between −2.8–3.2 kV; S-lens RF level at 40%, and heated metal capillary temperature at 350°C. Ions were initially accumulated in an external multipole ion guide (1–5 ms) and released dependently of mass to charge ratio (m/z) by controlled decrease of an auxiliary radio frequency potential between the multipole rods and the end-cap electrode (Kaiser et al., 2013). Ions were excited to m/z-dependent radius to maximize the dynamic range and number of observed mass spectral peaks (32%–64%) (Kaiser et al., 2013). Excitation and detection were performed with the same pair of electrodes (Chen et al., 2014). Time-domain transients of 3.1 s were initiated by a TTL trigger from the commercial Thermo data station and conditionally co-added and acquired with the Predator data station with 100 averaged time-domain acquisitions (Blakney et al., 2011). Mass spectra were phase-corrected (Xian et al., 2010) and internally calibrated with 10–15 highly abundant homologous series that span the entire molecular weight distribution based on the "walking" calibration method (Savory et al., 2011). Experimentally measured masses were converted from the International Union of Pure and Applied Chemistry mass scale to the Kendrick mass scale (Kendrick, 1963) for rapid identification of homologous series for each heteroatom class (i.e., species with the same $C_cH_hN_nO_oS_s$ content, differing only by degree of alkylation; hereafter referred to as CHO, CHON, CHOS, and CHONS) (Hughey et al., 2001). Peaks with signal magnitude greater than 6 times the baseline root-mean-square (rms) noise at m/z 400 were exported to peak lists, and molecular formula assignments and data visualization were performed with PetroOrg © software (Bahureksa et al., 2022; Corilo, 2015; Kim et al., 2003). Molecular formula assignments with an error >0.2 parts-per-million were discarded, and only chemical classes with a combined % RA of ≥0.15 were considered. Compound classes were defined based on elemental ratios and the modified aromaticity index (AI_{mod}); specifically, as highly

unsaturated polyphenolics (HUPs), low O/C ($AI_{mod} < 0.5$, H/C < 1.5, O/C < 0.5), HUPs, high O/C ($AI_{mod} < 0.5$, H/C < 1.5, O/C ≥ 0.5), aliphatic (H/C ≥ 1.5, $N = 0$), condensed aromatic ($AI_{mod} \geq 0.67$), polyphenolic ($0.67 > AI_{mod} > 0.5$), and peptide-like (H/C ≥ 1.5, $N > 0$). Contributions of each heteroatom and compound class to total composition were calculated as the sum of all the relative abundances (RA) of each peak in a given compound class divided by the summed abundances of all assigned formula and reported here as % RA. 21 T FT-ICR MS files and elemental compositions are openly available via the Open Science Framework at DOI 10.17605/OSF.IO/3R86F.

2.4. Statistical Analysis

Data were analyzed for normality using the Shapiro-Wilk test and for homogeneity of variance using Levene's test in R. The data were non-parametric and parameters were analyzed for significant differences using Kruskal-Wallis one-way analysis of variance test. Significant effects were assessed with Dunn's test for multiple comparisons with Bonferroni adjustment. Principal component analysis (PCA) was conducted using the "vegan" package in R (Oksanen et al., 2020). Results were considered significant where $p < 0.05$. Spearman's correlation analysis was performed between FT-ICR MS measured variables and BDOC loss.

3. Results

Inoculum did not significantly affect any measured variable based on the threshold of $p < 0.05$, therefore results for all parameters except BDOC loss (Figure 2) are presented as the average of all inoculum treatments for each stock and timepoint. Data for all treatment combinations is available in Table S1 in Supporting Information S1.

3.1. DOC Concentrations and BDOC Loss

Holocene permafrost stock had the lowest initial DOC concentration and the lowest BDOC loss, decreasing from 16.10 mg L^{-1} at T_0 to 12.00 ± 0.74 mg L^{-1} DOC at T_{100}, with a BDOC loss of −25.49% and an average k of 0.1 d^{-1} (Tables 1 and 2; Figure 2a). Pleistocene permafrost stock had the highest initial DOC concentration and the highest BDOC loss, decreasing from 173.63 mg L^{-1} at T_0 to 52.01 mg L^{-1} ± 1.96 at T_{100}, with an average BDOC loss of −70.05% and an average k of 0.22 $days^{-1}$ (Tables 1 and 2; Figure 2b). The shallow wetland stock had an initial DOC concentration of 48.49 mg L^{-1} and decreased to 23.22 ± 0.61 mg L^{-1} at T_{100}, exhibiting an average BDOC loss of −52.12% and an average k of 0.62 $days^{-1}$ (Tables 1 and 2; Figure 2c). The deep wetland stock decreased from 37.33 mg L^{-1} DOC on T_0 to 21.05 ± 0.78 mg L^{-1} DOC on T_{100}, with an average BDOC loss of −43.62% and an average k of 0.77 $days^{-1}$ (Tables 1 and 2; Figure 2d).

At T_0, the concentrations of DOC were significantly different between Pleistocene permafrost stock and all other treatments (Dunn's $p < 0.005$), as was Holocene permafrost DOC concentration and all other treatments (Dunn's $p < 0.005$). Deep and shallow wetland stock DOC did not differ significantly from each other (Dunn's $p = 0.22$). Similarly, BDOC loss varied significantly between stocks ($p < 0.05$), where Pleistocene permafrost stock had significantly higher percent loss than Holocene permafrost stock (Dunn's $p < 0.005$; −70.05 vs. −25.49%, Table 1). However, there were no significant differences between other stocks with regards to BDOC percent loss. The value of k varied significantly with stock ($p < 0.05$), with the Holocene permafrost stock having significantly lower k values than both wetland depth stocks (Dunn's $p < 0.05$, Table 2).

3.2. Initial DOM Composition Relationship to BDOC

Principal component analysis revealed distinct clustering separating Pleistocene samples from all other stocks, where Holocene and both wetland depth samples clustered toward the righthand quadrants regardless of the timepoint when they were sampled (Figure 3). Pleistocene samples, however, demonstrated a clear North-East shift across PC axes from the lefthand side at T_0 toward the upper right quadrant closer to the mid-point of PC1 at T_{100}. PC1 explained 63.6% of the variance and was driven negatively by aliphatic and peptide-like % RA and DOC concentration, and positively by AI_{mod} and the % RA of condensed aromatic and polyphenolic compound classes. PC2 explained 19.0% of the variance and was driven positively by CHONS and CHON % RA, and negatively by CHO and HUPs (Low O/C) % RA (Table S2 in Supporting Information S1).

The % RA of HUPs (High O/C) varied significantly with stock type ($p < 0.05$), where Pleistocene stock exhibited the lowest % RA of HUPS (High O/C) amongst all treatments (34.67% RA, Figure 4), and the % RA of HUPs

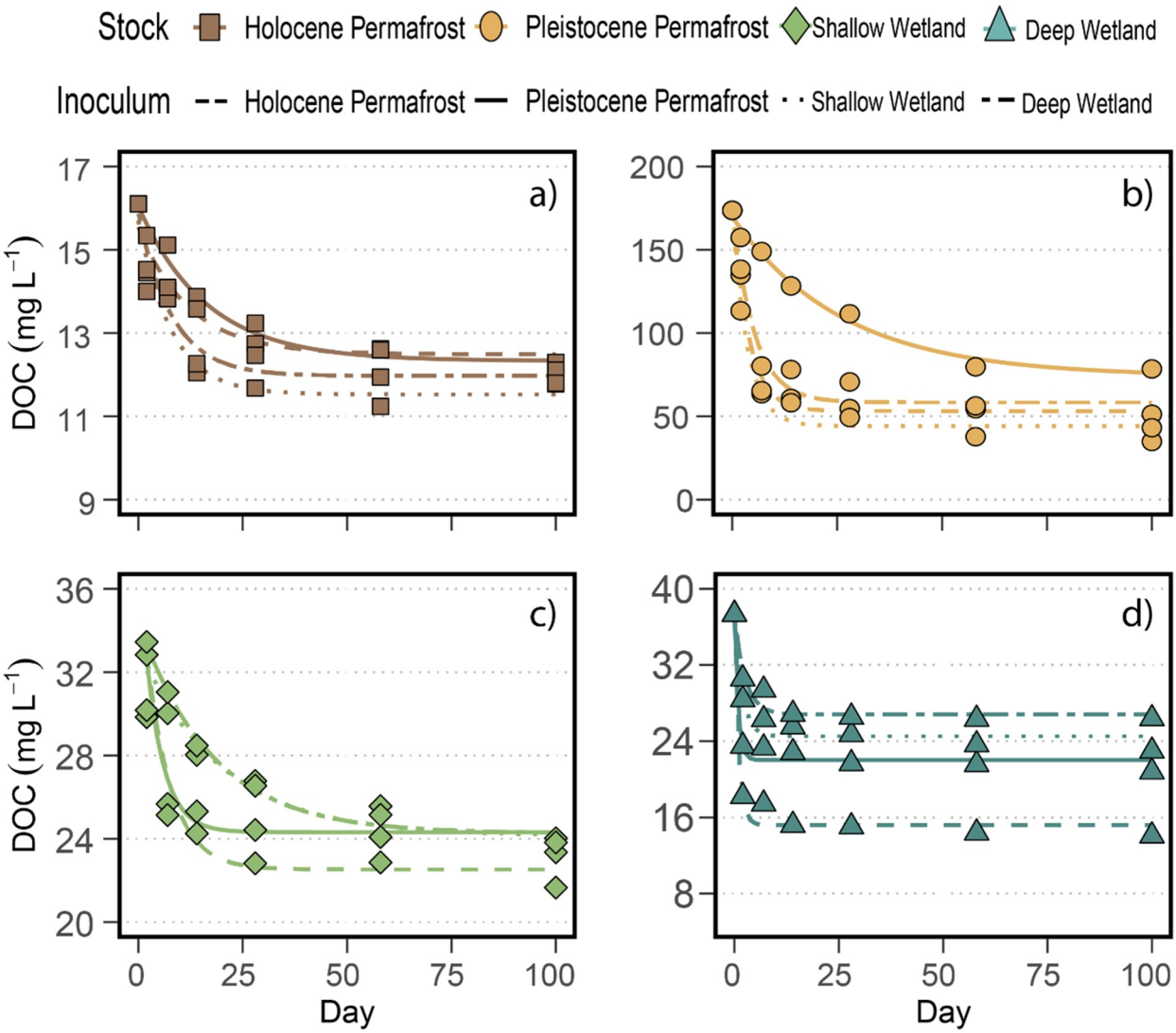

Figure 2. Loss of dissolved organic carbon (DOC) over time for: (a) Holocene permafrost stock, (b) Pleistocene permafrost stock, (c) shallow wetland stock, and (d) deep wetland stock. Points represent mean DOC concentrations of triplicate bioincubation samples at each time point for each treatment combination. Lines represent fit of a three-parameter exponential decay model as described in the methods. Pleistocene inoculum treatments are indicated by a solid line, Holocene inoculum by a dashed line, shallow wetland inoculum by a dotted line, and deep wetland inoculum by an alternating dashed line.

(Low O/C) was not significantly different between stocks at T_0 ($p = 0.47$). There was little to no correlation between HUPs (High O/C) and HUPs (Low O/C) and BDOC loss, respectively (Figure 5). The % RA of condensed aromatic and polyphenolic formula varied significantly between stock types ($p < 0.05$), with the lowest values observed in the Pleistocene permafrost treatments (Table 3; Figure 4). Both condensed aromatic and polyphenolic % RA clustered out along the right side of PC1 (Figure 3) and were strongly negatively correlated with BDOC loss (Figure 5). Similarly, the % RA of aliphatic and peptide-like compound classes were strongly positively correlated with BDOC loss (Figure 5) and clustered out on the left side of PC1 (Figure 3). Pleistocene stock had significantly higher % RA of both aliphatic and peptide-like compound classes than all other stock treatments ($p < 0.005$), which were all otherwise similar to each other in regards to both aliphatic and peptide-like formula (Table 3; Figure 4, Dunn's $p > 0.05$). Accordingly, BDOC loss was strongly correlated with AI_{mod} (Figure 5) which clusters with condensed aromatic and polyphenolic abundance on PC1 (Figure 3).

While CHO, CHON, or CHONS % RA accounted for the variance along PC2 (Figure 3), these parameters were not significantly correlated with BDOC loss, although there was a positive correlation between BDOC loss and CHOS (Figure 5). Stock type had a significant effect on CHO, CHON, CHOS, and CHONS % RA ($p < 0.005$) and

Table 1
DOC Concentration for Each Timepoint and BDOC Loss (Percent Change From T_0 to T_{100}) Over Time

Stock	Day	DOC (mg L^{-1})	S.D.	BDOC loss (%)
Holocene permafrost	0	16.10	–	–
Holocene permafrost	2	14.58	±0.99	–
Holocene permafrost	7	14.26	±0.65	–
Holocene permafrost	14	12.94	±1.03	–
Holocene permafrost	28	12.48	±0.64	–
Holocene permafrost	58	12.10	±1.05	–
Holocene permafrost	100	12.00	±0.74	−25.49
Pleistocene permafrost	0	173.63	–	–
Pleistocene permafrost	2	136.00	±2.67	–
Pleistocene permafrost	7	89.56	±2.51	–
Pleistocene permafrost	14	81.37	±2.00	–
Pleistocene permafrost	28	73.46	±3.45	–
Pleistocene permafrost	58	57.14	±2.20	–
Pleistocene permafrost	100	52.01	±1.96	−70.05
Shallow wetland	0	48.49	–	–
Shallow wetland	2	31.57	±0.57	–
Shallow wetland	7	27.97	±0.49	–
Shallow wetland	14	26.52	±0.62	–
Shallow wetland	28	25.63	±0.50	–
Shallow wetland	58	24.42	±0.80	–
Shallow wetland	100	23.22	±0.59	−52.12
Deep wetland	0	37.33	–	–
Deep wetland	2	25.15	±0.48	–
Deep wetland	7	24.08	±0.59	–
Deep wetland	14	22.58	±0.66	–
Deep wetland	28	22.05	±0.76	–
Deep wetland	58	21.47	±0.43	–
Deep wetland	100	21.05	±0.78	−43.62

Note. Results are presented here as the average of all inoculum treatments for each stock.

Pleistocene permafrost exhibited the lowest observed CHO % RA and the highest, CHON and CHOS % RA (Figure 6). The initial % RA of CHONS classed formula was lower than 2% across all treatments and was lowest in Pleistocene permafrost stocks (1.09% RA, Figure 6).

At T_0, H/C showed variability between stocks, with Pleistocene permafrost stock having the highest H/C value of all stocks (Table 3). Pleistocene initial H/C was significantly higher than in both the deep wetland and Holocene permafrost stocks (Dunn's p 0.05; Table 3, Figure 7), but the difference between the Pleistocene and shallow wetland initial H/C did not reach the threshold for statistical significance (Dunn's $p = 0.15$, Figure 7). O/C values at T_0 were also variable between stocks, with a significantly lower value in Pleistocene permafrost stock at T_0 than both wetland depth stocks and the Holocene permafrost stock (Dunn's $p < 0.05$; Figure 7) and with comparable values between the wetlands stocks and the Holocene permafrost stock (Figure 7). N/C ratios were ~0.02 across all treatments (Table 3, Table S1 in Supporting Information S1, Figure 7).

3.3. DOM Compositional Changes Through the Bioincubations

The % RA of HUPs (High O/C) increased over time in the Pleistocene stock and decreased slightly in the Holocene stock over the incubation period (Figure 4; Table 3), and this apparent decrease in the latter was once again driven by the Holocene stock/deep wetland inoculum treatment combination (Figure S1 in Supporting Information S1). There was little change in HUPs (High O/C) % RA in either wetland stock (Figure 4; Table 3). Low O/C HUPs % RA showed only marginal changes over the course of the bioincubation, with small increases in the Holocene and deep wetland stocks and small decreases in the Pleistocene and shallow wetland stocks (Figure 4; Table 3). The % RA of condensed aromatics increased across all stocks over the course of the bioincubation, with the greatest relative increase in Pleistocene and shallow wetland stocks (Figure 4; Table 3). The % RA of polyphenolic formula followed a similar trend to the condensed aromatics, where most stocks had an increase in polyphenolic % RA with the exception of the Holocene permafrost samples, which had almost no change (Figure 4; Table 3). Pleistocene permafrost stock had the greatest increase in polyphenolic % RA from T_0 to T_{100} from 9.56% to 12.75% RA. The % RA of aliphatic and peptide-like species decreased over time in Pleistocene samples from 24.80 to 5.84% RA and 5.15 to 1.78% RA, respectively (Figure 4; Table 3). Both wetland depth stocks also demonstrated decreasing aliphatic and peptide-like % RA over time, and there was a small increase in these species in the Holocene stock bioincubations (Figure 4; Table 3). Change in the % RA of all compound classes between T_0 and T_{100} for all stock/inoculum combinations is available in Figure S1 and Table S1 in Supporting Information S1.

There was almost no change in CHO % RA over the bioincubation period in most treatments, with the exception of a slight decrease in the Pleistocene treatments (Figure 6; Table 3). CHON % RA increased between T_0 and T_{100} in Pleistocene and shallow wetland samples, while Holocene and deep wetland bioincubations experienced minimal change (Figure 6; Table 3). All samples showed little change in CHOS % RA over time (Figure 6; Table 3). The % RA of CHONS more than doubled in Pleistocene bioincubations and showed minor increases in the other treatments (Figure 6; Table 3). Change in % RA of heteroatom composition between T_0 and T_{100} for all stock/inoculum combinations is available in Figure S2 and Table S1 in Supporting Information S1.

Between T_0 and T_{100}, H/C ratio decreased in Pleistocene stocks and shallow wetland stocks, with almost no change in either Holocene or deep wetland stocks (Figure 7; Table 3). Pleistocene stock O/C increased over the course of the bioincubation, and there was almost no change in either wetland stock (Figure 4; Table 3); the apparent decrease in Holocene O/C was driven by a decrease only in the Holocene stock/deep wetland inoculum

Table 2
Three-Parameter Exponential Decay Model for Each Stock/Inoculum Treatment Combination, Where k Is the First Order Rate Constant of DOC Loss Over Time

Stock/Inoculum	$C\infty$ (mg L^{-1})	z_o (mg L^{-1})	k (d^{-1})	r	p
Holocene/holocene	12.49	3.05	0.08	0.95	<0.05
Holocene/pleistocene	12.34	3.70	0.06	0.99	<0.05
Holocene/shallow	11.53	4.18	0.13	0.97	<0.05
Holocene/deep	11.97	3.89	0.12	0.97	<0.05
Pleistocene/holocene	53.26	123.67	0.26	0.99	<0.05
Pleistocene/pleistocene	61.50	109.41	0.17	0.81	<0.05
Pleistocene/shallow	44.20	127.12	0.27	0.99	<0.05
Pleistocene/deep	58.39	115.02	0.19	0.98	<0.05
Shallow/holocene	23.25	25.19	0.63	0.99	<0.05
Shallow/pleistocene	24.67	23.81	0.76	1.00	<0.05
Shallow/shallow	26.58	21.77	0.58	0.97	<0.05
Shallow/deep	26.73	21.49	0.51	0.97	<0.05
Deep/holocene	15.19	22.13	0.99	0.99	<0.05
Deep/pleistocene	22.01	15.31	1.17	0.99	<0.05
Deep/shallow	24.51	12.73	0.56	0.98	<0.05
Deep/deep	26.82	10.20	0.39	0.97	<0.05

treatment (Figure S3 and Table S1 in Supporting Information S1). N/C ratios did not change substantially over the course of the incubations in any treatment (Figure 7; Table 3). AI_{mod} increased across all samples between T_0 and T_{100}, with the largest increases observed in the Pleistocene and shallow wetland stocks (Figure 7; Table 3). Change in H/C, O/C, and N/C ratios and AI_{mod} between T_0 and T_{100} for all stock/inoculum combinations is available in Figure S3 and Table S1 in Supporting Information S1.

4. Discussion

4.1. Organic Matter Origin Controls BDOC Loss, Not Microbial Source

The source of inoculum (i.e., the fraction containing microbes from each leachate stock) had no statistically significant impact on BDOC loss from permafrost and wetland leachates across our experimental incubations. In other words, for any given leachate type, the addition of any of the four different inocula resulted in statistically similar DOC loss. Instead, stock type and its associated DOM composition was the dominant influence on the loss of DOC and the rate of biodegradation in the bioincubations. Pleistocene stock bioincubations experienced the greatest loss of DOC over 100 days, while Holocene stock exhibited the lowest BDOC loss (Table 1; Figure 2) and the lowest k value (Table 2), indicating relatively slow BDOC loss. Both shallow wetland and Pleistocene permafrost stocks exhibited a continual decrease in DOC concentration throughout the bioincubation period in most treatment combinations (Table 1; Figures 2b and 2c). While as much as 10 Tg yr^{-1} of DOC is estimated to be released from organic-rich Pleistocene permafrost deposits alone by 2100, the signal of Pleistocene permafrost thaw is often undetectable in downstream surface waters because its DOM

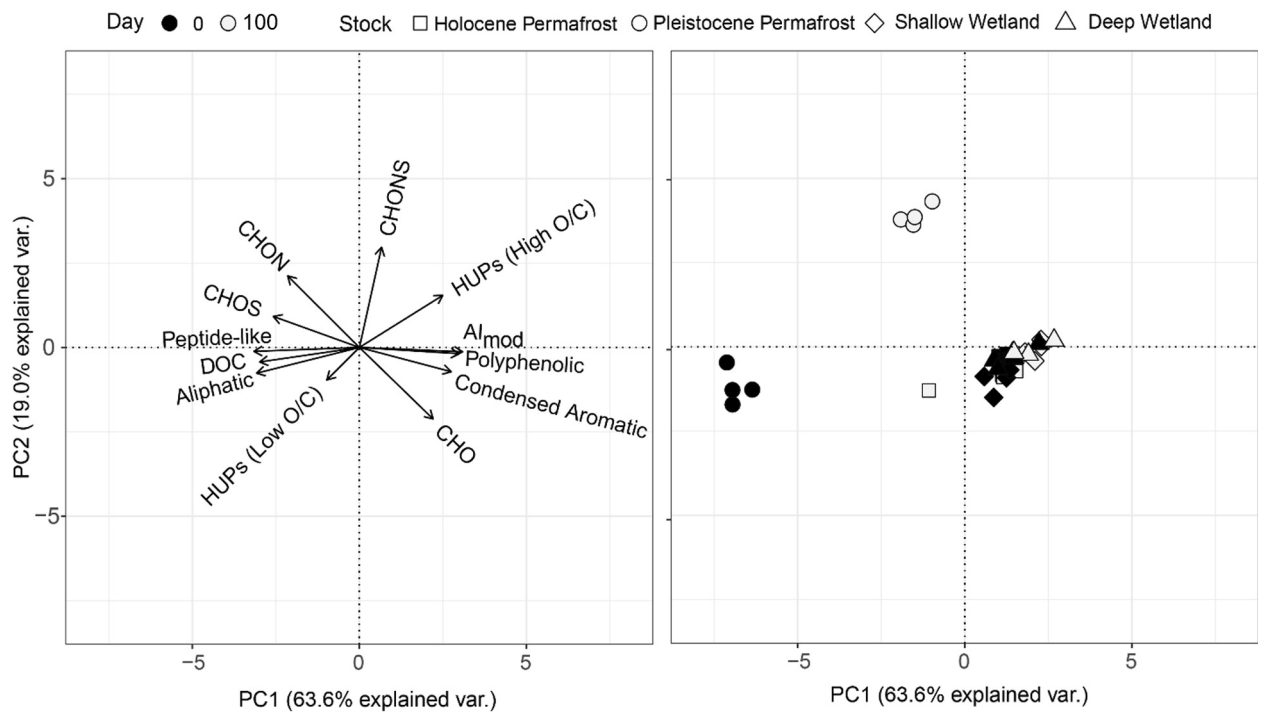

Figure 3. Principal component analysis of measured compositional parameters from the bioincubations. Loadings for each variable are plotted on the left and the individual samples at T_0 and T_{100} are plotted on the right, in black and white, respectively. Shape corresponds to stock treatment, with Holocene permafrost stock as squares, Pleistocene permafrost as circles, shallow wetland as diamonds, and deep wetland as triangles.

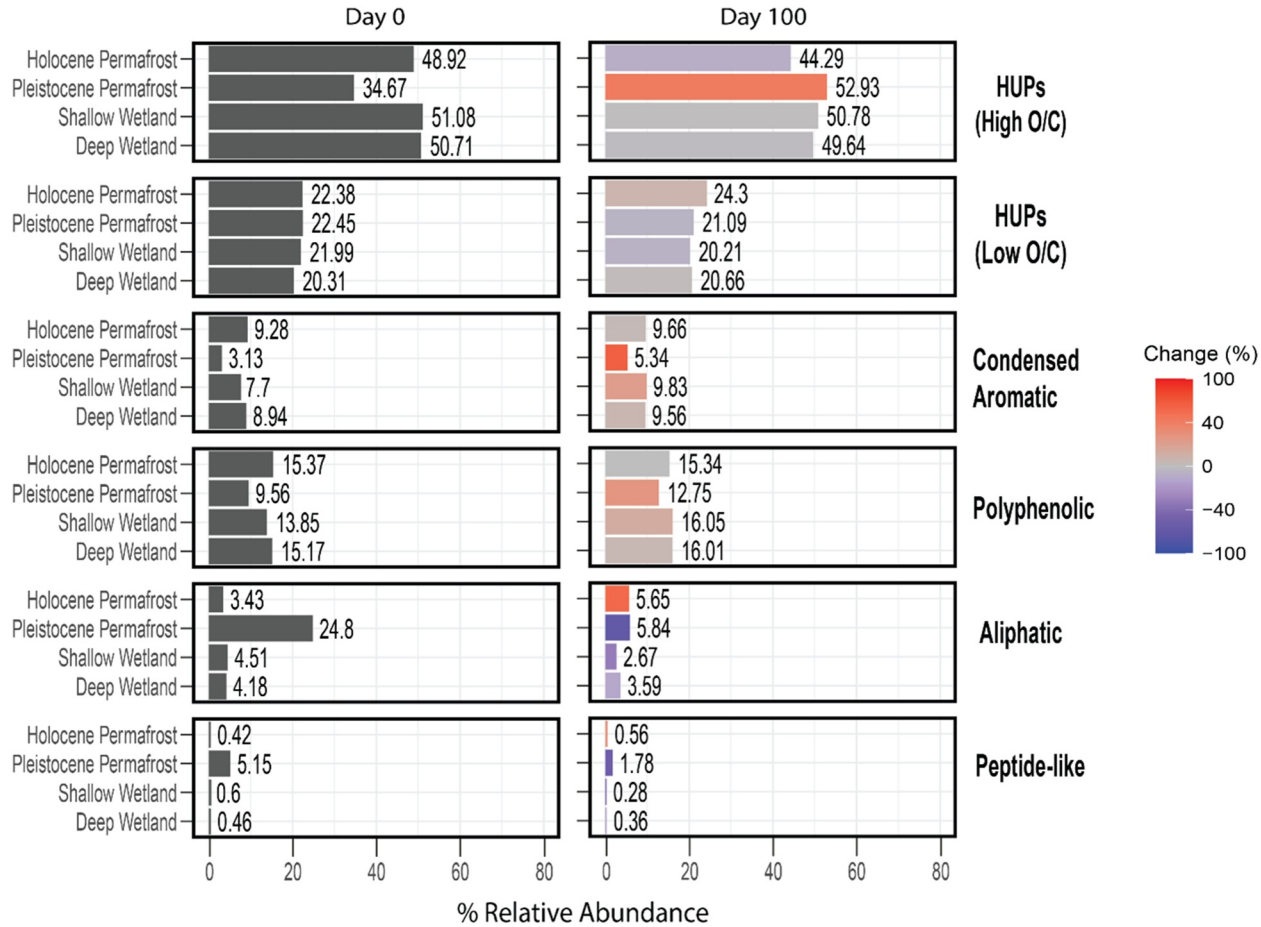

Figure 4. Average relative abundance (% RA) of compound class for each stock treatment at T_0 and T_{100}. The color scale for T_{100} represents the percent change in relative abundance between the final and beginning incubation measurements, where relative increases are shown in red and relative decreases are shown in blue. Results are presented here as the average of all inoculum treatments for each stock.

molecular composition favors rapid mineralization (Drake et al., 2015; Spencer et al., 2015). While our data agrees with previous predictions that permafrost DOC is highly bioavailable and rapidly degraded following thaw (Drake et al., 2015; Spencer et al., 2015), the continual degradation of DOC over the course of our 100-day bioincubation suggests that a small portion of biodegradable permafrost-derived DOC may persist in the environment at longer time scales than previously observed.

Previous bioincubation experiments observed as much as 50% loss of BDOC in Pleistocene-derived DOC (Vonk et al., 2015), occurring even as rapidly as 7 days (Spencer et al., 2015). However, these studies are constrained by relatively short incubation times. Critically, we observed approximately 70% BDOC loss across the Pleistocene permafrost incubations with different inocula, a higher percent loss than has been previously observed. However, at 7 days we observed an approximate 48% BDOC loss in Pleistocene stock treatments which is consistent with previous observations on those timelines (Drake et al., 2015; Spencer et al., 2015; Vonk et al., 2015). This observation, combined with the greater percent loss at 100 days, intermediate k value, and lack of observed asymptote in the decay curves of most of our treatment combinations (Figure 2b), suggests that the reactivity of these leachates may have been systematically underestimated due to the short bioincubations performed in these types of experiments and that Pleistocene permafrost deposit-derived DOM may continue to biodegrade in the environment on the scale of months.

The significant BDOC loss observed in Pleistocene permafrost under all experimental conditions indicates that permafrost-derived DOM is highly susceptible to microbial degradation, leading to potential greenhouse gas emissions. This challenges the notion that wetlands may effectively mitigate the release of DOM from thawing permafrost, as proposed by some studies (Heffernan et al., 2020; Holmes et al., 2022; Tanentzap et al., 2021).

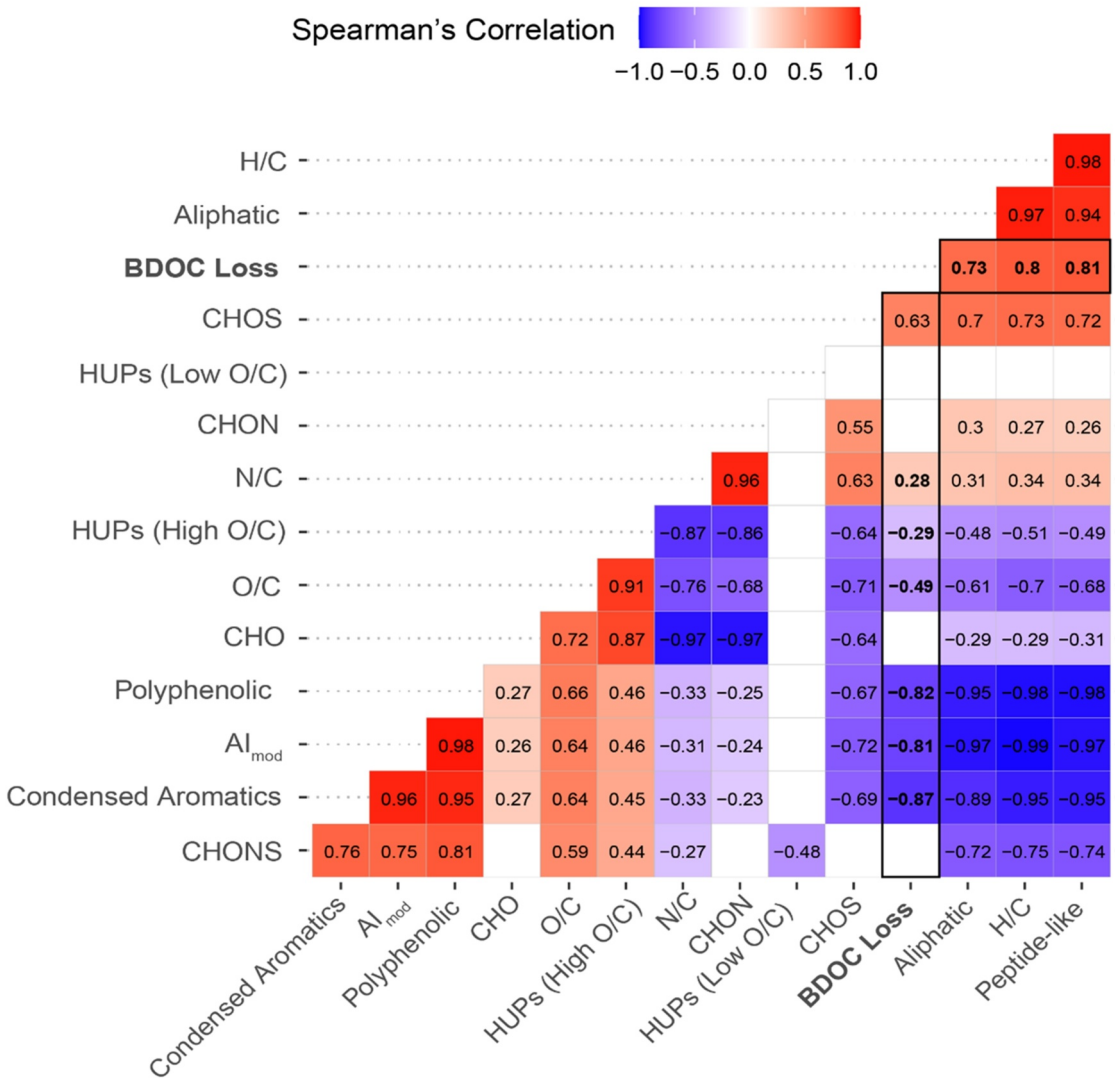

Figure 5. Correlogram showing Spearman's correlation coefficients between FT-ICR-measured variables and BDOC loss. BDOC loss coefficients are highlighted in bold. Non-significant results are omitted. Red squares correspond to positively correlated variables while blue squares represent negative correlations.

However, our aerobic bioincubations only reflect potential mixing of permafrost and wetland-derived DOM in oxygenated surface waters such as in a flowing fluvial environment. Under real-world conditions, wetlands adjacent to thawing permafrost may store DOM from permafrost inputs due to transport through inundated areas that slow the activity of aerobic microbial processes (Tanentzap et al., 2021), reducing the potential for greenhouse gas production from the mobilization of permafrost-derived DOM. Thus, under anaerobic conditions, it is possible that Pleistocene permafrost-derived DOM may experience less rapid BDOC loss (Schädel et al., 2016). Given that more than half of northern wetlands are currently permafrost-affected (Hugelius et al., 2020), in situ measurements are needed to understand the rate at which Pleistocene permafrost thaw impacts greenhouse gas fluxes in wetlands receiving DOM subsidies from these sources. Our results underscore the need to account for the diverse ecological processes that influence the fate of permafrost-derived DOM in different aquatic environments.

Results from this study confirm that the bioavailability of DOC from Arctic wetland and permafrost landscapes can be predicted from its DOM molecular-level composition. Interestingly, we found that older, Pleistocene permafrost-derived DOM was more bioavailable than younger Holocene permafrost DOM, consistent with previous observations of trends with depth, and subsequently age, in syngenetic permafrost cores (Ewing,

Table 3
Average FT-ICR MS Parameters for Each Stock Treatment at T_0 and T_{100}

	Holocene permafrost		Pleistocene permafrost		Shallow wetland		Deep wetland	
Variable	T_0	T_{100}	T_0	T_{100}	T_0	T_{100}	T_0	T_{100}
HUPs (High O/C) (% RA)	48.92	44.29	34.67	52.93	51.08	50.78	50.71	49.64
HUPs (Low O/C) (% RA)	22.38	24.30	22.45	21.09	21.99	20.21	20.31	20.66
Condensed aromatic (% RA)	9.28	9.66	3.13	5.34	7.70	9.83	8.94	9.56
Polyphenolic (% RA)	15.37	15.34	9.56	12.75	13.85	16.05	15.17	16.01
Aliphatic (% RA)	3.43	5.65	24.80	5.84	4.51	2.67	4.18	3.59
Peptide-like (% RA)	0.42	0.56	5.15	1.78	0.60	0.28	0.46	0.36
CHO (% RA)	66.74	67.06	61.92	57.87	70.30	68.86	68.87	68.88
CHON (% RA)	22.27	21.35	25.24	28.24	18.82	20.15	19.69	19.78
CHOS (% RA)	9.65	10.21	11.76	11.45	9.67	9.29	9.93	9.54
CHONS (% RA)	1.34	1.38	1.09	2.44	1.21	1.70	1.51	1.80
H/C	1.01	1.02	1.27	1.08	1.04	0.99	1.01	1.00
O/C	0.54	0.51	0.48	0.55	0.54	0.54	0.54	0.54
N/C	0.02	0.02	0.02	0.03	0.02	0.02	0.02	0.02
AI_{mod}	0.37	0.37	0.24	0.32	0.35	0.38	0.36	0.37

O'Donnell, et al., 2015). Specifically, DOM with a high % RA of aliphatic and peptide-like formula and/or high H/C ratio potentially has greater bioavailability than DOM relatively enriched in condensed aromatics and polyphenolics, with a high O/C ratio (Figures 3, 5, and 7; Table S2 in Supporting Information S1). These findings support the idea that the thaw of older sources, such as from Pleistocene-aged permafrost deposits, could lead to the rapid release of large amounts of bioavailable carbon, as suggested by previous research (Ewing, O'Donnell,

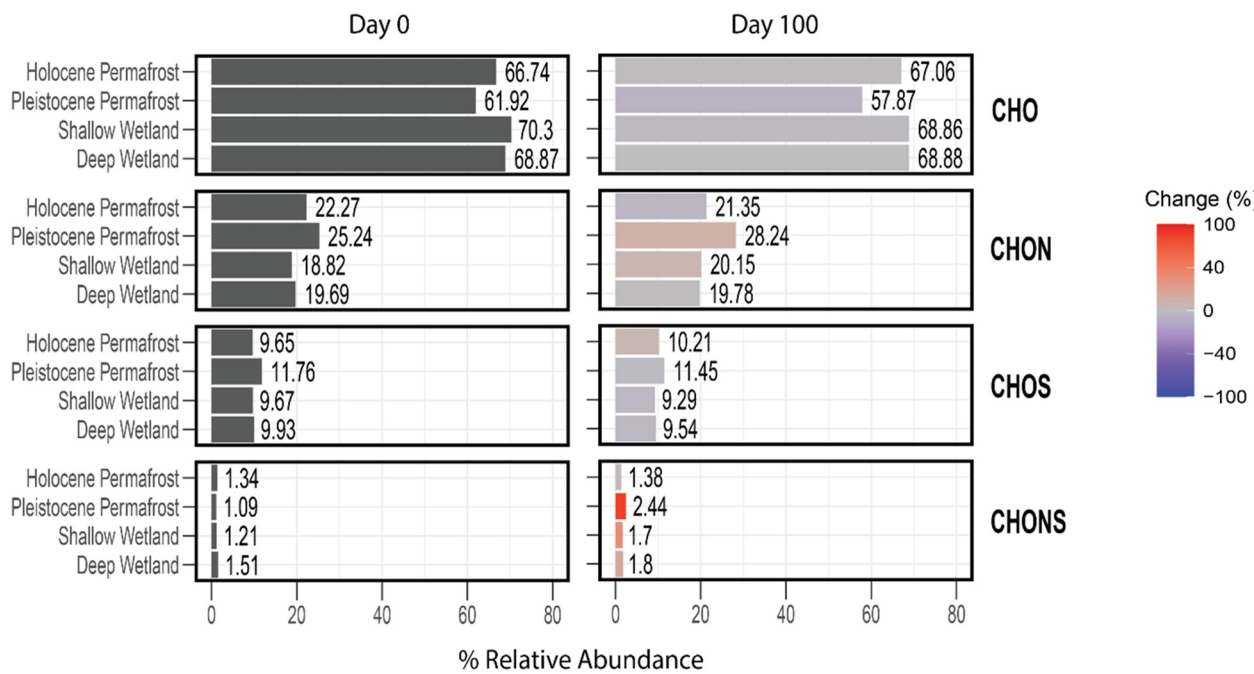

Figure 6. Average relative abundance (% RA) of elemental composition for each stock treatment at T_0 and T_{100}. The color scale for T_{100} represents the percent change in relative abundance between the final and beginning incubation measurements, where relative increases are shown in red and relative decreases are shown in blue. Results are presented here as the average of all inoculum treatments for each stock.

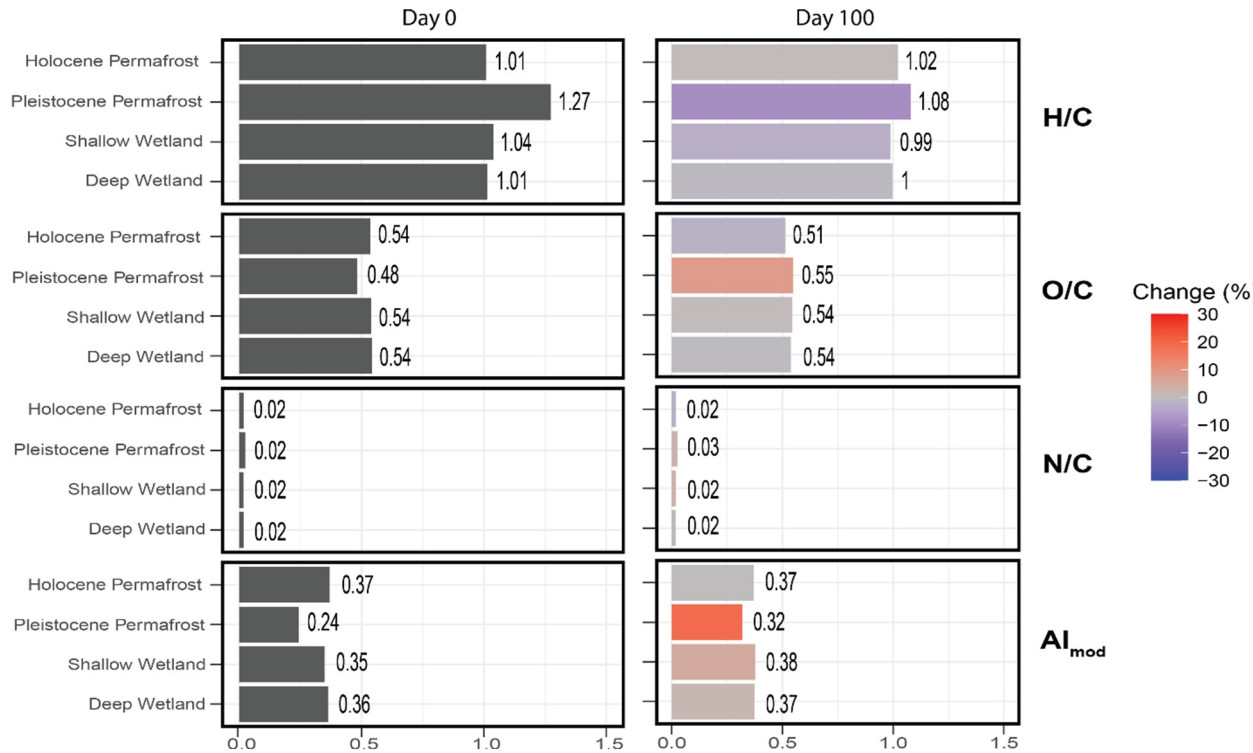

Figure 7. Average H/C, O/C, N/C, and AI_{mod} values for each stock treatment at T_0 and T_{100}. The color scale for T_{100} represents the percent change of each variable between the final and beginning incubations, where relative increases are shown in red and relative decreases are shown in blue. Results are presented here as the average of all inoculum treatments for each stock.

et al., 2015; Ewing, Paces, et al., 2015; Vonk et al., 2015). Crucially, the apparent age-dependency of bioavailability implies that as thaw progresses into deeper, older deposits, rates of carbon release to the atmosphere may accelerate.

4.2. Toward Stability: DOM Compositional Changes During Biodegradation

The PCA showed distinct differences between Pleistocene samples and the other stock types, with a marked shift in Pleistocene stock between timepoints (Figure 3; Table 3). Specifically, Pleistocene permafrost-derived DOM underwent readily apparent compositional changes over the course of the bioincubations. Specifically, H/C decreased while O/C, N/C and AI_{mod} increased and converged toward similar values to the other stocks at T_0 by the end of the bioincubation. High O/C HUPs, condensed aromatic and polyphenolic % RA all increased in the Pleistocene stocks as well, while the % RA of aliphatic and peptide-like species decreased (Figures 4 and 5; Table 3). These changes indicate a transformation of Pleistocene permafrost DOM from that of a strongly bioavailable composition toward a more stable signature apparently from microbial degradation. While there were slight changes in the composition of the DOM from the other stock treatments, none were as dramatic as observed in the Pleistocene stock. While BDOC loss occurred in these other treatment types, the compositional metrics we measured remained relatively stable over the course of our experimental incubations relative to the degree of change in the Pleistocene stock (Figures 4, 6, and 7). This suggests that the DOM sourced from the other soil types is more stable with respect to compositional change resulting from microbial degradation within our experimental window, despite BDOC losses of 25%–52% or is driven by loss of organic matter outside the analytical window of FT-ICR MS.

While the DOM composition of the Holocene permafrost stock showed slight increases in aliphatic and peptide-like species abundance (Figure 4), these increases appear to be driven by the Holocene stock/deep wetland inoculum treatment combination (Figure S1 and Table S1 in Supporting Information S1). Given the statistical insignificance of inoculum treatment across all measured parameters, we consider this to be an outlier. When this treatment combination is removed, there appears to be little change in the composition of Holocene DOM over the

course of our bioincubations, and such stability reflects the relatively low BDOC loss from Holocene stock treatments compared with the other stock types. Thus, we propose that DOC released into aquatic ecosystems from some thawing Holocene-age deposits may be relatively stable and potentially available to be transported downstream.

While we had hypothesized that deeper wetland soils would have lower bioavailability and a more stable compositional DOM signature, there was little difference in the DOM composition between shallow and deep wetland samples with the exception of CHONS % RA, which comprised less than 2% of the RA of all four heteroatom classes, and there was little change in DOM composition in either wetland stock treatment over the course of the bioincubations. However, the apparent continuation of BDOC loss in the shallow wetland stocks versus the relatively rapid plateau of BDOC loss in the deep wetland stocks suggests that DOC from different wetland soil depths could diverge in composition during processing on longer timescales. The similarity in DOM composition in our wetland treatments may also be a result of the sampling focused on relatively shallow soils; our deep wetland soils were collected from only 15–30 cm depths, whereas previous studies have shown marked differences in composition and reactivity between surface peat and layers beyond 50 cm (Lin et al., 2012; Tfaily et al., 2014, 2018).

4.3. Future Considerations and Conclusions

The experimental design had the benefit of isolating interactions between microbial inocula and DOM composition from environmental factors like temperature changes and variable redox conditions. However, both biological and abiotic environmental effects may alter the processing of DOM from wetland and permafrost soils in natural systems. Additionally, our findings are based on soils from a single region of Alaska and may not be representative of systems across the Arctic; especially given the variability of conditions within and amongst wetland types. Differences in soil types and physicochemistry, hydrological regimes, and vegetation in northern ecosystems will impact DOM processing dynamics across both space and time. Thus, in situ observations are needed to determine the impact of such environmental influences on BDOC loss in these ecosystems. Moreover, assessing biogeochemical dynamics in wetland soils can be particularly difficult because redox conditions, nutrient availability, and hydrology can vary dramatically not only between different wetland types but even at finer scales; sometimes differing substantially from meter to meter within a single site. Given the widely varying conditions across wetlands, the effects we observed from the treatments utilizing fen soils may not apply to other wetland types. Furthermore, while the absence of microbial inoculum source effects observed in our study has implications in understanding the interactions between microbial community structure and ecological function, explicit measurement of microbial community structure and microbial biomass in similar bioincubation experiments should be conducted to further elucidate the impact of microbial diversity on BDOC loss in northern ecosystems.

Our data also highlight the need for increased bioincubation length in future studies. In our bioincubations, BDOC loss in some treatments effectively stopped after the first 3 weeks, specifically in the Holocene and deep wetland stocks. The fit of decay curves in most of the Pleistocene stock treatments appeared to stabilize by day 28 with the exception of the Pleistocene stock/Pleistocene inoculum treatment which continued to decrease until day 60. However, the individual DOC concentration measurements for all shallow wetland stocks and most Pleistocene permafrost stocks continued to decrease from day 56 to day 100 (Figure 2). While the majority of permafrost and wetland-derived DOM biodegradation occurs rapidly, these findings suggest that a portion of BDOC transformation may remain unobserved on the timescales used in most bioincubation experiments.

Warming Arctic permafrost deposits are predicted to release large amounts of DOC by 2100, and ice-rich Pleistocene-aged deposits are at particularly high risk for thaw and subsequent OC release; 210–500 Pg C are estimated to be stored in organic-rich Pleistocene permafrost deposits alone (Miner et al., 2022; Zimov et al., 2006). Our results confirm that Pleistocene permafrost-derived DOM is highly bioavailable and thus subject to rapid mineralization during transport, suggesting that the majority of DOC released by permafrost thaw will likely contribute to further warming feedbacks. Through FT-ICR MS we have demonstrated that DOM composition is a strong driver of BDOC loss in these systems and microbial source did not have a significant effect on BDOC loss or DOM transformation in our experimental incubations. Additionally, we found that while Pleistocene permafrost contained the most bioavailable DOM, the DOM from the upper 30 cm of wetland soil is also readily available for biodegradation. Furthermore, in areas where wetland and permafrost-derived DOC can

mix on the landscape, we found that this biodegradation can occur regardless of microbial source. These findings offer insight into the processing and fate of DOC released by northern soils under continued warming that will be critical in informing future carbon budgets under a changing Arctic landscape.

Conflict of Interest

The authors declare no conflicts of interest relevant to this study.

Data Availability Statement

All data, including 21 T FT-ICR MS files and elemental compositions, are openly available via the Open Science Framework at https://doi.org/10.17605/OSF.IO/3R86F (Starr et al., 2025).

Acknowledgments
Special thanks to Suzi Arzoumanyan for assistance with sample collection and processing. Any use of trade, firm, or product names is for descriptive purposes only and does not imply endorsement by the U.S. Government. This research was supported by NSF-DEB 2029585 to RGMS, NSF-DEB 2029573 to RM, NSF-DEB-202930 to ALS, and NSF Graduate Research Fellowship and INTERN awards to SFS. A portion of this work was performed at the National High Magnetic Field Laboratory ICR User Facility, which is supported by the National Science Foundation Division of Chemistry and Division of Materials Research through DMR-1644779 and the State of Florida.

References

Bahureksa, W., Borch, T., Young, R. B., Weisbrod, C. R., Blakney, G. T., & McKenna, A. M. (2022). Improved dynamic range, resolving power, and sensitivity achievable with FT-ICR mass spectrometry at 21 T reveals the hidden complexity of natural organic matter. *Analytical Chemistry*, *94*(32), 11382–11389. https://doi.org/10.1021/ACS.ANALCHEM.2C02377

Behnke, M. I., McClelland, J. W., Tank, S. E., Kellerman, A. M., Holmes, R. M., Haghipour, N., et al. (2021). Pan-Arctic riverine dissolved organic matter: Synchronous molecular stability, shifting sources and subsidies. *Global Biogeochemical Cycles*, *35*(4), e2020GB006871. https://doi.org/10.1029/2020GB006871

Blakney, G. T., Hendrickson, C. L., & Marshall, A. G. (2011). Predator data station: A fast data acquisition system for advanced FT-ICR MS experiments. *International Journal of Mass Spectrometry*, *306*(2–3), 246–252. https://doi.org/10.1016/J.IJMS.2011.03.009

Boldin, I. A., & Nikolaev, E. N. (2011). Fourier transform ion cyclotron resonance cell with dynamic harmonization of the electric field in the whole volume by shaping of the excitation and detection electrode assembly. *Rapid Communications in Mass Spectrometry*, *25*(1), 122–126. https://doi.org/10.1002/RCM.4838

Chanton, J. P., Glaser, P. H., Chasar, L. S., Burdige, D. J., Hines, M. E., Siegel, D. I., et al. (2008). Radiocarbon evidence for the importance of surface vegetation on fermentation and methanogenesis in contrasting types of boreal peatlands. *Global Biogeochemical Cycles*, *22*(4). https://doi.org/10.1029/2008GB003274

Chaudhary, N., Westermann, S., Lamba, S., Shurpali, N., Sannel, A. B. K., Schurgers, G., et al. (2020). Modelling past and future peatland carbon dynamics across the pan-Arctic. *Global Change Biology*, *26*(7), 4119–4133. https://doi.org/10.1111/GCB.15099

Chen, T., Beu, S. C., Kaiser, N. K., & Hendrickson, C. L. (2014). Note: Optimized circuit for excitation and detection with one pair of electrodes for improved Fourier transform ion cyclotron resonance mass spectrometry. *Review of Scientific Instruments*, *85*(6). https://doi.org/10.1063/1.4883179

Corilo, Y. E. (2015). *PetroOrg software*. Florida State University. All Rights reserved. 8.

D'Andrilli, J., Chanton, J. P., Glaser, P. H., & Cooper, W. T. (2010). Characterization of dissolved organic matter in northern peatland soil porewaters by ultra high resolution mass spectrometry. *Organic Geochemistry*, *41*(8), 791–799. https://doi.org/10.1016/j.orggeochem.2010.05.009

Dittmar, T., Koch, B., Hertkorn, N., & Kattner, G. (2008). A simple and efficient method for the solid-phase extraction of dissolved organic matter (SPE-DOM) from seawater. *Limnology and Oceanography: Methods*, *6*(6), 230–235. https://doi.org/10.4319/LOM.2008.6.230

Drake, T. W., Wickland, K. P., Spencer, R. G. M., McKnight, D. M., & Striegl, R. G. (2015). Ancient low-molecular-weight organic acids in permafrost fuel rapid carbon dioxide production upon thaw. *Proceedings of the National Academy of Sciences of the United States of America*, *112*(45), 13946–13951. https://doi.org/10.1073/pnas.1511705112

Druckenmiller, M. L., Thoman, R. L., & Moon, T. A. (2022). Arctic report card 2022. https://doi.org/10.25923/YJX6-R184

Elder, C., Hasson, N., Hanke, P., Wright, S., Walter Anthony, K., & Miller, C. E. (2021). *Methane fluxes from shorelines and differing surfaces, big Trail Lake, Alaska, 2019*. ORNL DAAC.

Emmett, M. R., White, F. M., Hendrickson, C. L., Shi, D. H., & Marshall, A. G. (1998). Application of micro-electrospray liquid chromatography techniques to FT-ICR MS to enable high-sensitivity biological analysis. *Journal of the American Society for Mass Spectrometry*, *9*(4), 333–340. https://doi.org/10.1016/S1044-0305(97)00287-0

Ewing, S. A., O'Donnell, J. A., Aiken, G. R., Butler, K., Butman, D., Windham-Myers, L., & Kanevskiy, M. Z. (2015). Long-term anoxia and release of ancient, labile carbon upon thaw of Pleistocene permafrost. *Geophysical Research Letters*, *42*(24). https://doi.org/10.1002/2015GL066296

Ewing, S. A., Paces, J. B., O'Donnell, J. A., Kanevskiy, M. Z., Shur, Y., Jorgenson, M. T., et al. (2015). Uranium isotopes and dissolved organic carbon in loess permafrost: Modeling the age of ancient ice. *Geochimica et Cosmochimica Acta*, *152*, 143–165. https://doi.org/10.1016/j.gca.2014.11.008

Frey, K. E., & McClelland, J. W. (2009). Impacts of permafrost degradation on arctic river biogeochemistry. *Hydrological Processes*, *23*(1), 169–182. https://doi.org/10.1002/hyp.7196

Frey, K. E., & Smith, L. C. (2005). Amplified carbon release from vast West Siberian peatlands by 2100. *Geophysical Research Letters*, *32*(9), 1–4. https://doi.org/10.1029/2004GL022025

Hamilton, T. D., Craig, J. L., & Sellmann, P. V. (1988). The Fox permafrost yunnel: A late Quaternary geologic record in central Alaska. *Geological Society of America Bulletin*, *100*(6), 948–969. https://doi.org/10.1130/0016-7606(1988)100<0948:tfptal>2.3.co;2

Harden, J. W., Fuller, C. C., Wilmking, M., Meyers-Smith, I. H., Trumbore, S. E., & Bubier, J. (2008). The fate of terrestrial carbon following permafrost degradation: Detecting changes over recent decades. *Proceedings of Ninth International Conference on Permafrost*, *29*, 649–654.

Heffernan, L., Estop-Aragonés, C., Knorr, K. H., Talbot, J., & Olefeldt, D. (2020). Long-term impacts of permafrost thaw on carbon storage in peatlands: Deep losses offset by surficial accumulation. *Journal of Geophysical Research: Biogeosciences*, *125*(3), e2019JG005501. https://doi.org/10.1029/2019JG005501

Hendrickson, C. L., Quinn, J. P., Kaiser, N. K., Smith, D. F., Blakney, G. T., Chen, T., et al. (2015). 21 Tesla Fourier transform ion cyclotron resonance mass spectrometer: A national resource for ultrahigh resolution mass analysis. *Journal of the American Society for Mass Spectrometry*, *26*(9), 1626–1632. https://doi.org/10.1007/s13361-015-1182-2

Hodgkins, S. B., Tfaily, M. M., Podgorski, D. C., McCalley, C. K., Saleska, S. R., Crill, P. M., et al. (2016). Elemental composition and optical properties reveal changes in dissolved organic matter along a permafrost thaw chronosequence in a subarctic peatland. *Geochimica et Cosmochimica Acta*, *187*, 123–140. https://doi.org/10.1016/j.gca.2016.05.015

Holmes, M. E., Crill, P. M., Burnett, W. C., McCalley, C. K., Wilson, R. M., Frolking, S., et al. (2022). Carbon accumulation, flux, and fate in Stordalen Mire, a permafrost peatland in transition. *Global Biogeochemical Cycles*, *36*(1), e2021GB007113. https://doi.org/10.1029/2021GB007113

Holmes, R. M., Coe, M. T., Fiske, G. J., Gurtovaya, T., McClelland, J. W., Shiklomanov, A. I., et al. (2013). Climate change impacts on the hydrology and biogeochemistry of Arctic rivers. *Climatic change and global warming of inland waters*, 1–26. https://doi.org/10.1002/9781118470596.ch1

Hugelius, G., Loisel, J., Chadburn, S., Jackson, R. B., Jones, M., MacDonald, G., et al. (2020). Large stocks of peatland carbon and nitrogen are vulnerable to permafrost thaw. *Proceedings of the National Academy of Sciences of the United States of America*, *117*(34), 20438–20446. https://doi.org/10.1073/PNAS.1916387117

Hughey, C. A., Hendrickson, C. L., Rodgers, R. P., Marshall, A. G., & Qian, K. (2001). Kendrick mass defect spectrum: A compact visual analysis for ultrahigh-resolution broadband mass spectra. *Analytical Chemistry*, *73*(19), 4676–4681. https://doi.org/10.1021/AC010560W

Jiao, N., Herndl, G. J., Hansell, D. A., Benner, R., Kattner, G., Wilhelm, S. W., et al. (2010). Microbial production of recalcitrant dissolved organic matter: Long-term carbon storage in the global ocean. *Nature Reviews Microbiology*, *8*(8), 593–599. https://doi.org/10.1038/nrmicro2386

Johnson, J. B., & Lorenz, R. D. (2000). Thermophysical properties of Alaskan loess: An analog material for the Martian polar layered terrain? *Geophysical Research Letters*, *27*(17), 2769–2772. https://doi.org/10.1029/1999gl011077

Johnston, S. E., Shorina, N., Bulygina, E., Vorobjeva, T., Chupakova, A., Klimov, S. I., et al. (2018). Flux and seasonality of dissolved organic matter from the Northern Dvina (Severnaya Dvina) River, Russia. *Journal of Geophysical Research: Biogeosciences*, *123*(3), 1041–1056. https://doi.org/10.1002/2017JG004337

Kaiser, N. K., McKenna, A. M., Savory, J. J., Hendrickson, C. L., & Marshall, A. G. (2013). Tailored ion radius distribution for increased dynamic range in FT-ICR mass analysis of complex mixtures. *Analytical Chemistry*, *85*(1), 265–272. https://doi.org/10.1021/AC302678V

Kanevskiy, M., Shur, Y., Bigelow, N. H., Bjella, K. L., Douglas, T. A., Fortier, D., et al. (2022). Yedoma cryostratigraphy of recently excavated sections of the CRREL permafrost tunnel near Fairbanks, Alaska. *Frontiers in Earth Science*, *9*, 758800. https://doi.org/10.3389/feart.2021.758800

Kendrick, E. (1963). A mass scale based on CH2 = 14.0000 for high resolution mass spectrometry of organic compounds. *Analytical Chemistry*, *35*(13), 2146–2154. https://doi.org/10.1021/AC60206A048/ASSET/AC60206A048.FP.PNG_V03

Kicklighter, D. W., Hayes, D. J., Mcclelland, J. W., Peterson, B. J., Mcguire, A. D., & Melillo, J. M. (2013). Insights and issues with simulating terrestrial DOC loading of Arctic river networks. *Ecological Applications*, *23*(8), 1817–1836. https://doi.org/10.1890/11-1050.1

Kim, S., Kramer, R. W., & Hatcher, P. G. (2003). Graphical method for analysis of ultrahigh-resolution broadband mass spectra of natural organic matter, the van Krevelen diagram. *Analytical chemistry*, *75*(20), 5336–5344. https://doi.org/10.1021/ac034415p

Klanten, Y., Couture, R. M., Christoffersen, K. S., Vincent, W. F., & Antoniades, D. (2023). Oxygen depletion in Arctic lakes: Circumpolar trends, biogeochemical Processes, and implications of climate change. *Global Biogeochemical Cycles*, *37*(5), e2022GB007616. https://doi.org/10.1029/2022GB007616

Kuhn, M. A., Varner, R. K., Bastviken, D., Crill, P., MacIntyre, S., Turetsky, M., et al. (2021). BAWLD-CH 4: A comprehensive dataset of methane fluxes from boreal and arctic ecosystems. *Earth System Science Data Discussions*, *2021*(11), 1–56. https://doi.org/10.5194/essd-13-5151-2021

Lin, X., Green, S., Tfaily, M. M., Prakash, O., Konstantinidis, K. T., Corbett, J. E., et al. (2012). Microbial community structure and activity linked to contrasting biogeochemical gradients in bog and fen environments of the glacial lake agassiz peatland. *Applied and Environmental Microbiology*, *78*(19), 7023–7031. https://doi.org/10.1128/AEM.01750-12/SUPPL_FILE/ZAM999103710SO1.PDF

Mackelprang, R., Burkert, A., Haw, M., Mahendrarajah, T., Conaway, C. H., Douglas, T. A., & Waldrop, M. P. (2017). Microbial survival strategies in ancient permafrost: Insights from metagenomics. *The ISME journal*, *11*(10), 2305–2318. https://doi.org/10.1038/ismej.2017.93

Miner, K. R., Turetsky, M. R., Malina, E., Bartsch, A., Tamminen, J., David McGuire, A., et al. (2022). Permafrost carbon emissions in a changing Arctic. *Nature Reviews Earth & Environment*, *3*(1), 55–67. https://doi.org/10.1038/s43017-021-00230-3

Mohammed, A. A., Guimond, J. A., Bense, V. F., Jamieson, R. C., McKenzie, J. M., & Kurylyk, B. L. (2022). Mobilization of subsurface carbon pools driven by permafrost thaw and reactivation of groundwater flow: A virtual experiment. *Environmental Research Letters*, *17*(12), 124036. https://doi.org/10.1088/1748-9326/ACA701

Moore, M. R. N., Tank, S. E., Kurek, M. R., Taskovic, M., McKenna, A. M., Smith, J. L. J., et al. (2023). Ultrahigh resolution dissolved organic matter characterization reveals distinct permafrost characteristics on the Peel Plateau, Canada. *Biogeochemistry*, *167*(2), 1–19. https://doi.org/10.1007/s10533-023-01101-3

Natali, S. M., Holdren, J. P., Rogers, B. M., Treharne, R., Duffy, P. B., Pomerance, R., & MacDonald, E. (2021). Permafrost carbon feedbacks threaten global climate goals. *Proceedings of the National Academy of Sciences*, *118*(21), e2100163118. https://doi.org/10.1073/PNAS.2100163118

Ni, M., & Li, S. (2023). Ultraviolet humic-like component contributes to riverine dissolved organic matter biodegradation. *Journal of Environmental Sciences*, *124*, 165–175. https://doi.org/10.1016/J.JES.2021.10.011

Oksanen, J., Blanchet, F. G., Friendly, M., Kindt, R., Legendre, P., Mcglinn, D., et al. (2020). *Package "vegan" title community ecology package version 2.5-7*. Retrieved from http://cran.ism.ac.jp/web/packages/vegan/vegan.pdf

Perreault, N., Lévesque, E., Fortier, D., Gratton, D., Lamarque, L. J., Perreault, N., et al. (2017). Remote sensing evaluation of High Arctic wetland depletion following permafrost disturbance by thermo-erosion gullying processes 1. *Arctic Science*, *3*, 237–253. https://doi.org/10.1139/as-2016-0047

Phoenix, G. K., & Treharne, R. (2022). Arctic greening and browning: Challenges and a cascade of complexities. *Global Change Biology*, *28*(11), 3481–3483. https://doi.org/10.1111/GCB.16118

Pokrovsky, O. S., Manasypov, R. M., Loiko, S., Shirokova, L. S., Krickov, I. A., Pokrovsky, B. G., et al. (2015). Permafrost coverage, watershed area and season control of dissolved carbon and major elements in western Siberian rivers. *Biogeosciences*, *12*(21), 6301–6320. https://doi.org/10.5194/bg-12-6301-2015

Savory, J. J., Kaiser, N. K., McKenna, A. M., Xian, F., Blakney, G. T., Rodgers, R. P., et al. (2011). Parts-per-billion Fourier transform ion cyclotron resonance mass measurement accuracy with a "walking" calibration equation. *Analytical chemistry*, *83*(5), 1732–1736. https://doi.org/10.1021/ac102943z

Schädel, C., Bader, M. K. F., Schuur, E. A., Biasi, C., Bracho, R., Čapek, P., et al. (2016). Potential carbon emissions dominated by carbon dioxide from thawed permafrost soils. *Nature Climate Change*, *6*(10), 950–953. https://doi.org/10.1038/nclimate3054

Schuur, E. A. G., Abbott, B. W., Commane, R., Ernakovich, J., Euskirchen, E., Hugelius, G., et al. (2022). Permafrost and climate change: Carbon cycle feedbacks from the warming Arctic. *Annual Review of Environment and Resources*, *47*(1), 343–371. https://doi.org/10.1146/ANNUREV-ENVIRON-012220-011847

Schuur, E. A. G., Bockheim, J., Canadell, J. G., Euskirchen, E., Field, C. B., Goryachkin, S. V., et al. (2008). Vulnerability of permafrost carbon to climate change: Implications for the global carbon cycle. *BioScience*, *58*(8), 701–714. https://doi.org/10.1641/b580807

Smith, D. F., Podgorski, D. C., Rodgers, R. P., Blakney, G. T., & Hendrickson, C. L. (2018). 21 Tesla FT-ICR mass spectrometer for ultrahigh-resolution analysis of complex organic mixtures. *Analytical Chemistry*, *90*(3), 2041–2047. https://doi.org/10.1021/acs.analchem.7b04159

Speetjens, N. J., Hugelius, G., Gumbricht, T., Lantuit, H., Berghuijs, W. R., Pika, P. A., et al. (2023). The pan-Arctic catchment database (ARCADE). *Earth System Science Data*, *15*(2), 541–554. https://doi.org/10.5194/essd-15-541-2023

Spencer, R. G. M., Mann, P. J., Dittmar, T., Eglinton, T. I., McIntyre, C., Holmes, R. M., et al. (2015). Detecting the signature of permafrost thaw in Arctic rivers. *Geophysical Research Letters*, *42*(8), 2830–2835. https://doi.org/10.1002/2015GL063498

Starr, S., Johnston, S. E., Sobolev, N., Perminova, I., Kellerman, A., Fiske, G., et al. (2023). Characterizing uncertainty in Pan-Arctic land-ocean dissolved organic carbon flux: Insights from the Onega River, Russia. *Journal of Geophysical Research: Biogeosciences*, *128*(5), e2022JG007073. https://doi.org/10.1029/2022JG007073

Starr, S., Wickland, K. P., Kellerman, A. M., McKenna, A. M., Kurek, M. R., Miller, A., et al. (2025). Organic matter composition versus microbial source: Controls on carbon loss in wetland and permafrost environments [Dataset]. *OSF*. https://doi.org/10.17605/OSF.IO/3R86F

Sun, L., Perdue, E. M., Meyer, J. L., & Weis, J. (1997). Use of elemental composition to predict bioavailability of dissolved organic matter in a Georgia river. *Limnology & Oceanography*, *42*(4), 714–721. https://doi.org/10.4319/LO.1997.42.4.0714

Takano, S., Yamashita, Y., Tei, S., Liang, M., Shingubara, R., Morozumi, T., et al. (2021). Stable water isotope assessment of tundra wetland hydrology as a potential source of Arctic riverine dissolved organic carbon in the Indigirka River Lowland, Northeastern Siberia. *Frontiers in Earth Science*, *9*, 699365. https://doi.org/10.3389/FEART.2021.699365

Tanentzap, A. J., Burd, K., Kuhn, M., Estop-Aragonés, C., Tank, S. E., & Olefeldt, D. (2021). Aged soils contribute little to contemporary carbon cycling downstream of thawing permafrost peatlands. *Global Change Biology*, *27*(20), 5368–5382. https://doi.org/10.1111/GCB.15756

Tank, S. E., Vonk, J. E., Walvoord, M. A., McClelland, J. W., Laurion, I., & Abbott, B. W. (2020). Landscape matters: Predicting the biogeochemical effects of permafrost thaw on aquatic networks with a state factor approach. *Permafrost and Periglacial Processes*, *31*(3), 358–370. https://doi.org/10.1002/ppp.2057

Tfaily, M. M., Cooper, W. T., Kostka, J. E., Chanton, P. R., Schadt, C. W., Hanson, P. J., et al. (2014). Organic matter transformation in the peat column at Marcell Experimental Forest: Humification and vertical stratification. *Journal of Geophysical Research: Biogeosciences*, *119*(4), 661–675. https://doi.org/10.1002/2013JG002492

Tfaily, M. M., Hamdan, R., Corbett, J. E., Chanton, J. P., Glaser, P. H., & Cooper, W. T. (2013). Investigating dissolved organic matter decomposition in northern peatlands using complimentary analytical techniques. *Geochimica et Cosmochimica Acta*, *112*, 116–129. https://doi.org/10.1016/j.gca.2013.03.002

Tfaily, M. M., Wilson, R. M., Cooper, W. T., Kostka, J. E., Hanson, P., & Chanton, J. P. (2018). Vertical stratification of peat pore water dissolved organic matter composition in a Peat Bog in Northern Minnesota. *Journal of Geophysical Research: Biogeosciences*, *123*(2), 479–494. https://doi.org/10.1002/2017JG004007

Turetsky, M. R. (2004). Decomposition and organic matter quality in continental peatlands: The ghost of permafrost past. *Ecosystems*, *7*(7), 740–750. https://doi.org/10.1007/s10021-004-0247-z

Vonk, J. E., Tank, S. E., Mann, P. J., Spencer, R. G. M., Treat, C. C., Striegl, R. G., et al. (2015). Biodegradability of dissolved organic carbon in permafrost soils and aquatic systems: A meta-analysis. *Biogeosciences*, *12*(23), 6915–6930. https://doi.org/10.5194/bg-12-6915-2015

Walter Anthony, K., Lindgren, P., Hanke, P., Engram, M., Anthony, P., Daanen, R. P., et al. (2021). Decadal-scale hotspot methane ebullition within lakes following abrupt permafrost thaw. *Environmental Research Letters*, *16*(3), 035010. https://doi.org/10.1088/1748-9326/abc848

Walter Anthony, K., Schneider von Deimling, T., Nitze, I., Frolking, S., Emond, A., Daanen, R., et al. (2018). 21st-century modeled permafrost carbon emissions accelerated by abrupt thaw beneath lakes. *Nature Communications*, *9*(1), 3262. https://doi.org/10.1038/s41467-018-05738-9

Walvoord, M. A., Kurylyk, B. L., Walvoord, M. A., & Zone, V. (2016). Hydrologic impacts of thawing permafrost-A review. *Review and Analysis*, *15*(6), 1–20. https://doi.org/10.2136/vzj2016.01.0010

Wickland, K. P., Neff, J. C., & Aiken, G. R. (2007). Dissolved organic carbon in Alaskan boreal forest: Sources, chemical characteristics, and biodegradability. *Ecosystems*, *10*(8), 1323–1340. https://doi.org/10.1007/s10021-007-9101-4

Wickland, K. P., Waldrop, M. P., Aiken, G. R., Koch, J. C., Jorgenson, M. T., & Striegl, R. G. (2018). Dissolved organic carbon and nitrogen release from boreal Holocene permafrost and seasonally frozen soils of Alaska. *Environmental Research Letters*, *13*(6), 065011. https://doi.org/10.1088/1748-9326/aac4ad

Xian, F., Hendrickson, C. L., Blakney, G. T., Beu, S. C., & Marshall, A. G. (2010). Automated broadband phase correction of Fourier transform ion cyclotron resonance mass spectra. *Analytical Chemistry*, *82*(21), 8807–8812. https://doi.org/10.1021/AC101091W

Zhou, C., Liu, Y., Liu, C., Liu, Y., & Tfaily, M. M. (2019). Compositional changes of dissolved organic carbon during its dynamic desorption from hyporheic zone sediments. *Science of the Total Environment*, *658*, 16–23. https://doi.org/10.1016/J.SCITOTENV.2018.12.189

Zimov, S. A., Schuur, E. A., & Chapin, F. S. F. S., III. (2006). Permafrost and the global carbon budget. *Science*, *312*(5780), 1612–1613. https://doi.org/10.1126/science.1128908